Investigation of a SiC/Ti-24Al-11Nb Composite

P.K. Brindley, P.A. Bartolotta,
and S.J. Klima
Lewis Research Center
Cleveland, Ohio

NASA

INVESTIGATION OF A SiC/Ti-24Al-11Nb COMPOSITE

P.K. Brindley, P.A. Bartolotta, and S.J. Klima
National Aeronautics and Space Administration
Lewis Research Center
Cleveland, Ohio 44135

SUMMARY

A summary of on-going research on the characterization of a continuous-fiber reinforced SiC/Ti-24Al-11Nb (at %) composite is presented. The powder metallurgy fabrication technique is described as are the nondestructive evaluation results of the as-fabricated composite plates. Tensile properties of the SiC fiber, the matrix material, and the 0° SiC/Ti-24Al-11Nb composite (fibers oriented unidirectionally, parallel to the loading axis) from room temperature to 1100 °C are presented and discussed with regard to the resultant fractography. The as-fabricated fiber-matrix interface has been examined by scanning transmission electron microscopy and the compounds present in the reaction zone have been identified. Fiber-matrix interaction and stability of the matrix near the fiber is characterized at 815, 985 and 1200 °C from 1 to 500 hr. Measurements of the fiber-matrix reaction, the loss of C-rich coating from the surface of the SiC fiber, and the growth of the β depleted zone in the matrix adjacent to the fiber are presented. These data and the difference in coefficient of thermal expansion between the fiber and matrix are discussed in terms of their likely effects on mechanical properties.

INTRODUCTION

There are ever increasing demands to develop low density materials that maintain high strength and stiffness properties at elevated temperatures. Such materials are essential if advances are to be realized in air and space travel. Continuous-fiber-reinforced intermetallic matrix composites are currently being investigated as one possible avenue to obtain material advances beyond the current state-of-the-art materials, namely, nickel-base superalloys. Aluminides were chosen (ref. 1) as candidate matrix materials because of their generally high melting points, which is expected to correlate to increases in use temperature; their low density; and their generally good oxidation resistance resulting from high aluminum contents. Intermetallics often exist over a wide range of chemical composition and frequently have solubility for substitutional third element additions such as may be useful in tailoring the microstructure to develop a more optimum matrix material.

Ti-24Al-11Nb (at %) was chosen for use as a matrix material because it exhibited several of the positive attributes listed above. In the temperature regime of interest, it is a two-phase material consisting of the DO_{19} hexagonal Ti_3Al (α_2) phase in a body centered cubic (β) matrix which has a high melting point of approximately 1500 °C (refs. 2) and a low density calculated to be

E-4253

5.1g/cc. Ti_3Al has good oxidation resistance only up to approximately 700 °C (ref. 3). However, a primary advantage of Ti_3Al is that it has been success-fully alloyed with Nb to develop ductility at low temperatures (refs. 4 to 6). Many intermetallics do not exhibit ductility at low temperatures due to the material's ordered atomic structure (ref. 7). This is true of unalloyed Ti_3Al as well as shown in figure 1. Lipsitt, Shechtman, and Shafrik (ref. 8) measured an average reduction-in-area (RA) of 0.1 percent at room temperature for single phase Ti_3Al. However, an increased ductility of 1.1 percent RA was observed at room temperature when additions of 5 at % Nb and 1 at % W were made. Both Moxson and Friedman (ref. 5) and Yolton, et al., (ref. 6) reported even further increases in ductility, with an average RA of 2.2 percent when 11 at % Nb was added to Ti_3Al. Also evident from figure 1 is the increased duc-tility present in all three materials at 700 °C.

Sastry and Lipsitt (ref. 9) have examined single phase Ti_3Al with approxi-mately 5 at % Nb in solution and compared its dislocation structure to that of single phase Ti_3Al to determine the role of Nb in attaining low temperature ductility. They found a-type super dislocations in the basal plane bound by four partials of the type $a/6<10\bar{1}0>$ in Ti_3Al and observed c-type dislocations only occasionally. The dislocations were observed in planar bands and disloca-tion walls. With the addition of 5 at % Nb, an increase in ductility was observed which they attributed to a reduction in the planarity of slip and increased nonbasal slip activity.

Further increases in Nb lead to a change in microstructure to two phase $\alpha_2 + \beta$ as shown in the psuedobinary Ti_3Al-Nb phase diagram (ref. 2) of fig-ure 2. The contribution of the β phase to improved ductility in Ti_3Al-Nb is not well understood. Although no direct evidence is available, P.L. Martin, et al., (ref. 4) and E.M. Schulson (ref. 10.) have indirectly attributed the observed increase in ductility with addition of Nb to a refinement in slip length. Slip length refinement was proposed due to observations of microstructural refinement with stabilization of the β phase.

Continuous fibers were chosen for reinforcement of the aluminides because they offer the largest potential benefits in increased modulus and strength as compared to particulate or chopped fiber reinforcement. The elastic modulus and ultimate tensile strength (UTS) of some of the currently available fibers varies from 380 GPa and 4150 MPa, respectively, for SiC fibers (refs. 11 and 12) to 825 GPa and 2250 MPa, respectively, for graphite fibers (Private communication with M. Townes of Amoco Performance Products, Parma, Ohio.). A plot of strength/density versus temperature for some of the currently avail-able fibers is shown in figure 3. Included are the SCS-6 fiber manufactured by Textron, formerly named Avco, (refs. 12 and 13); graphite fibers manufac-tured by Amoco; PRD-166 Al_2O_3-ZrO_2 and FP Al_2O_3 made by DuPont (ref. 14); sin-gle crystal Al_2O_3 manufactured by Saphikon (unpublished research of M.H. Jaskowiak of Lewis); and a W-Re-Hf-C fiber made on an experimental basis by Rhenium Alloys (ref. 15) for NASA Lewis Research Center. The various test en-vironments and test conditions are listed beside each set of data to point out that variability of properties can be incurred depending upon test condi-tions. Also indicated is the nominal fiber diameter of each material. Based upon this comparison, the SiC SCS-6 fiber was chosen as the first fiber rein-forcement to examine with the Ti-24Al-11Nb matrix because it offered the best strength/density properties of available fibers and because this 140 μm diame-ter, single-strand fiber was easily incorporated in the composite fabrication technique described below.

This paper provides the summary of on-going research on the characterization of a SiC/Ti-24Al-11Nb composite. The powder metallurgy fabrication technique, the method used for nondestructive evaluation of the composite, and the scanning transmission electron microscopy (STEM) preparation techniques will be described. Tensile properties of the SiC fiber, the matrix material, and the 0° SiC/Ti-24Al-11Nb composite tested over a range of temperatures will be presented and discussed with regard to the resultant fractography. The compounds comprising the reaction zone have been identified. Fiber-matrix interaction, stability of the matrix near the fiber, and stability of the C-rich coating on the SiC fiber surface will also be discussed. These compositional variations and the difference in coefficient of thermal expansion between the fiber and matrix are discussed in terms of their likely effects on mechanical properties.

EXPERIMENTAL PROCEDURE

A. Composite Fabrication

A powder cloth technique was used to fabricate SiC/Ti-24Al-11Nb composites as schematically illustrated in figure 4. Ti-24Al-11Nb cast electrodes were converted by the PREP process into powder. This prealloyed powder was blended with Teflon powder and stoddard solution and heated slowly to drive off the excess stoddard which was required for even blending. The powder mixture was then rolled to a desired thickness and cut to shape.

Fiber mats were made by turning the SiC fiber onto a mandrel at the desired-spacing and spraying it with a binder such an polystyrene. The fibers could then be cut to shape and handled easily.

The composite was arranged in alternating layers of powder cloth and fiber mat. Although any desired fiber orientation can be achieved, the present study involved only 0° fiber orientation. Heat and pressure were applied in a vacuum such that the binders were driven off during the consolidation cycle. Composite plates typically 5 cm by 1.5 mm were fabricated in this manner as shown in figure 5 and contained approximately 40 vol % fiber.

B. Nondestructive Evaluation

Microfocus radiography was used based on previously established procedures for ceramics (ref. 16). The self-contained microfocus radiography unit used in this investigation contained in a 60 kV X-ray tube, a molybdenum target and a mylar window. The effective focal spot size (source of X-rays) was nominally 10 μm. Projection radiographs were made by positioning the specimen so that the entire width was in the field of view with the film sufficiently far away to produce the desired magnification in the radiograph. The small focal spot made it possible to obtain magnified images with optimal geometric sharpness. Three types of images were possible with the microfocus system. A TV camera with an X-ray sensitive vidicon was moved into receiving position for real time radiography. Specimens could be quickly scanned for gross defects and rotated to obtain information regarding defect geometry. Radiographs were also made on instant print film as well as on fine grained radiographic film (Kodak type M.) Microfocus projection radiographs made on fine grained film

produced the best resolution of fiber fracture and porosity. Exposure param-
eters for the latter ranged from 40 to 60 kV for 5 to 20 min at 0.25 mA.

C. Tensile Tests

Specimens were tested under a positive pressure of He in a furnace which
was not sealed from the atmosphere at temperatures ranging from 23 to 1200 °C
for the SCS-6 fibers and from 23 to 1100 °C for the matrix-only and composite
specimens. Fiber tests included a minimum of 3 fibers at each temperature.
For the composite and the matrix-only data, 1 to 3 tests were run at each tem-
perature as will be indicated in the figures. In all cases, a strain rate of
1×10^{-4} s^{-1} was employed. Fracture surfaces were examined using a scanning
electron microscope (SEM).

D. Fiber-Matrix Reaction

Samples for STEM analysis were prepared at ALCOA Laboratories (Private
communication with S.D. Smith of Alcoa Laboratories, Alcoa Center, PA) by the
following procedure. Rectangular sections 1 by 25 mm were cut from a compos-
ite coupon using a thin diamond wheel. The sections were then immersed in a
nickel electroplating solution (ref. 17) to increase the composite thickness
dimension to a minimum of 2 mm for easier handling. Wafers 0.3 mm thick were
cut from the sections perpendicular to the fiber length using a thin diamond
wheel and then polished to approximately 0.25 mm using SiC paper. The wafers
were dimpled to obtain perforation, mounted on a cold stage, and ion milled at
5 kV and 2 mA. A tilt angle of 12° was used and the total milling time was
approximately 5 hr.

Coupons of SiC/Ti-24Al-11Nb were also annealed in vacuum over periods of 1
to 100 hr at 985 and 1200 °C and 1 to 500 hr at 815 °C in order to determine
the extent of fiber-matrix chemical reaction. Reaction zone thicknesses, the
SiC fiber's outer C-rich coating and the depletion of β within the matrix
adjacent to the fibers were measured from SEM micrographs at 10 to 20 kX magni-
fication. Each data point is an average of a minimum of 30 measurements and
the maximum standard deviation of the data plotted is indicated on each figure.

RESULTS AND DISCUSSION

A. Composite Fabrication

To ensure that the binders had been removed during consolidation, chemical
analysis was performed and the results are shown in table I. In particular,
C, H, and F were monitored since these comprised the major elements of the bin-
ders. F was generally detected at less than 0.025 at % (0.001 wt %), which
was the limit-of-detection of the equipment used, and occasionally was as high
as 0.0040 at % (0.0016 wt %). The H level appeared to have decreased in the
as-fabricated condition as compared to the starting matrix powder. The C level
indicated in table 1 was from the matrix consolidated without the SiC fiber so
as to reflect only the C remaining from the Teflon binder. These data were
sufficient to determine that both the Teflon and the polystyrene have been sat-
isfactorily removed during consolidation. Note also in table I the differences
in oxygen content of the two batches of prealloyed Ti-24Al-11Nb powder. The

first batch, indicated as High Oxygen, contained 0.332 at % (0.110 wt %) oxygen, while the second batch, indicated as Low Oxygen contained only 0.175 at % (0.059 wt %) oxygen. The importance of the oxygen content will be discussed later with respect to mechanical properties. Oxygen pickup during composite fabrication ranges from 0.031 to 0.121 at % (0.01-0.04 wt %) as shown in table I, and appears to make the powder cloth technique competitive with other powder metallurgy fabrication methods.

A transverse section of the as-fabricated 40 vol % SiC/Ti-24Al-11Nb composite is shown in figure 6 to illustrate typical fiber distribution and full matrix consolidation. The fiber volume fraction in composite tensile specimens ranged from 33.5 percent to 43.5 percent. Note that the 10 μm cladding present on the outside surface of the composite was removed mechanically before testing. Figure 7 is a single-fiber view of the transverse section which shows the fully-consolidated, two-phase matrix in which α_2 is the major constituent surrounded by β; the region encircling the fiber which is depleted of β; the 2 μm fiber-matrix reaction which developed during fabrication; and the C-rich coating of the SCS-6 SiC fiber (ref. 12) which appears as a black ring at the fiber's edge.

B. Nondestructive Evaluation

Microfocus radiography has been determined capable of detecting fiber breakage in these 3- and 4-fiber ply SiC/Ti-24Al-11Nb composites. In general, very little fiber damage was incurred during processing. However, when fiber breakage was observed, it was generally confined to the ends of a plate as shown in figure 8. The lower density SiC fibers appeared as vertical white bands and the higher density Ti-24Al-11Nb matrix appeared as the remaining gray and dark regions. Close examination of broken fibers such as at location "A" revealed mating fracture surfaces separated by a dark region in which matrix material has apparently infiltrated during consolidation.

Large regions of porosity, on the order of several fiber diameters or greater, were also detectable via microfocus radiography. However, porosity on a fine scale was not detectable, i.e., porosity located between two closely spaced fibers due to incomplete matrix consolidation. Therefore, metallographic sections of composite plates were used to determine fabrication parameters which produced full consolidation of the composite and microfocus radiography was used to detect gross porosity if a faulty vacuum hot press cycle was incurred. Microfocus radiography has thus been useful in characterizing the quality of the as-fabricated composite plates and for mapping out regions from which to machine test specimens.

C. Tensile Properties

Tensile properties at temperature for the SiC fiber, the Ti-24Al-11Nb matrix and the SiC/Ti-24Al-11Nb composite normalized to 40 vol % fiber are presented in figure 9. Average fiber values and the corresponding scatter bands are plotted. Rule-of-Mixtures (ROM) predictions based on fiber strength, the matrix strength, and 40 vol. % fiber are also included for comparison. The maximum and minimum fiber strength were used to calculate the upper and lower bounds of the ROM predictions. The actual composite strengths obtained were within the ROM range predicted in the intermediate temperature regime of 200 to 400 °C. At both room temperature and above 650 °C, however, composite

strengths were less-than-predicted. Note that the ROM range plotted in figure 9 does not reflect calculations between 650 and 1100 °C since matrix specimens were not tested between these two temperatures.

These data were generated without adequate strain measurements and therefore only the effect of temperature on the ultimate tensile strength is presented. We are currently repeating these tests with new instrumentation so as to obtain accurate modulus and strain-to-failure information. Table 2 contains the elastic modules (E) values obtained to date for SiC/Ti-24Al-11Nb at room temperature and 425 °C. Average E values of 220 GPa at room temperature and 208 GPa at 425°C were measured. Based on load versus crosshead extension plots, plasticity was exhibited for test temperatures at and above 200 °C.

The less-than-predicted room temperatures composite strength results of figure 9 are thought to be due to impurity contamination. It is known that impurities such as oxygen and carbon can embrittle intermetallic compounds (ref. 18). In this first generation of SiC/Ti-Al-11Nb composites, the oxygen level was approximately 0.332 at % (0.110 wt %) in the starting powder as shown in Table 1 and 0.453 at % (0.150 wt %) oxygen was present in the as-fabricated composite. It was therefore thought that the high oxygen content was responsible for the low composite strengths at room temperature by causing cracking at low strains within the matrix and subsequently propagation through the brittle fibers, not allowing the SiC fibers to attain their full strength potential. This proposed mode of failure was further supported by the lack of ductile features on the room temperature fracture surfaces as shown in figure 10(a), as well as the overall flat fracture appearance visible in figure 11(a) at room temperature in which the fibers and matrix failed in the same plane. It is expected the room temperature strength of this composite can be improved in the next generation of materials which start with powders with an average oxygen content of 0.175 at % (0.059 wt %). As shown in table I, the as-fabricated composite contains only 0.206 to 0.221 at % (0.069 to 0.074 wt %) oxygen, which is roughly half that of the first generation of composites.

With regard to the less-than-predicted strengths at 650 °C and above, two features were observed on the fracture surfaces: debonding and fiber pullout. Figure 10(b) and (c) shows the presence and location of debonding which occurred at the fiber/fiber coating interface and the fiber coating/matrix interface during elevated temperature tests. It is not clear from the present data how the reaction zone was involved when separation occurred at the fiber coating/matrix interface; e.g., did the reaction zone remain with the fiber, with the matrix, or with both? Surface analysis work is required to discern the nature of this interface. However, for the present discussion this interface will be referred to as the fiber coating/matrix interface. At room temperature, the bond between the fiber and matrix appears to remain intact. At 650 °C and above, the matrix separated from the C-rich coating of the fiber. Separation of the C-rich coating from the SiC fiber was sometimes observed in addition to the separation at the fiber coating/matrix interface as shown in figure 10(b) at 650 °C.

The seemingly intact bond at room temperature could have resulted from the formation of an adequate chemical bond between the fiber and matrix during fabrication. It could also be due to the matrix mechanically gripping the fibers (ref. 19) as the matrix contracts to a greater extent upon cooldown from the fabrication temperature than do the fibers (see the coefficients of thermal

6

expansion for SiC and Ti-24A1-11Nb plotted in fig. 21). Bonding at room tem-
perature could also be due to a combination of both the chemical and mechani-
cal effects.

Debonding in the presence of stress at elevated temperature would be
expected if the chemical bond were weak or if the bonding were primarily
mechanical. A fiber-matrix reaction zone with a low strain-to failure could
result in debonding due to tensile loading and/or due to the radial tensile
stress imposed on the interface as the matrix tries to expand at elevated tem-
peratures. The matrix expansion at elevated temperatures would also be ·
expected to reduce the frictional force exerted on the fiber by the matrix and
could help provide for fiber-matrix debonding in the presence of stress.

Fiber pullout was also observed in the elevated temperature fracture sur-
faces of the SiC/Ti-24-11Nb as shown in figure 11. Note that very little
fiber pullout was evident at room temperature and that increasing amounts of
fiber pullout were present as test temperature was increased. Again, lack of
fiber pullout at room temperature would be expected if there existed a strong
fiber-matrix chemical and/or mechanical bond. Fiber pullout at elevated tem-
perature would be expected to be aided by the difference in CTE of the fiber
and matrix following the reasoning above for debonding at elevated tempera-
tures. These conditions would be expected to result in fiber pullout as ran-
dom fiber breaks occurred throughout the test section.

The same thermal conditions and CTE mismatch conditions which lead to
debonding would also be expected to lead to fiber pullout since a weak bond
(chemical or mechanical) would be required for initiation of each. These
observations suggested that the less-than-ROM-predicted strengths for the
SiC/Ti-24-11Nb composite at elevated temperature resulted from a weak fiber-
matrix bond. Here, a weak bond is defined as one which cannot withstand the
imposed tensile stress in combination with the stresses induced by the twofold
difference in CTE of the SiC fiber and the Ti-24A1-11Nb matrix. Furthermore,
it is conceivable that the interfacial bond strength due to chemical interac-
tion could have been able to withstand higher tensile stresses under less
severe CTE mismatch conditions. The effects of a two- to fourfold difference
in CTE between currently available fibers and intermetallic matrices on compos-
ite properties will be discussed in more detail below.

To illustrate the potential for intermetallic matrix composites, the pre-
liminary tensile properties of SiC/Ti-24-11Nb were plotted on a strength/den-
sity basis versus temperature and compared to a range of wrought Ni-base
superalloys and to a single crystal Ni-base superalloy in figure 12. For this
first generation of composites, the 0° tensile properties met or exceeded
those of Ni-base superalloys. This provides the incentive to continue working
with intermetallic matrix composites, designing them such that they can exceed
existing materials properties by having the required directional properties
for a given application.

D. Fiber-Matrix Reaction

STEM analysis of the fiber-matrix chemical reaction products has revealed
two concentric zones, defined by the presence of carbides, within the
as-fabricated reaction zone as schematically illustrated in figure 13
(ref. 20). The zone adjacent to the fiber (zone 1) contained (Ti,Nb)C and

the zone adjacent to the matrix (zone 2) contained $(Ti,Nb)_3AlC$. A hexagonal Si-bearing phase was found throughout both zones and was characterized as $(Ti,Nb)_5Si_3$. In addition, fine porosity on the order of 0.01 μm was observed in zone 1 and a band of coarser porosity (~0.1 μm) was located near the center of zone 1. It is probable that the coarser band of porosity coincides with the original fiber-matrix interface before consolidation. Work is on-going with the as-recieved SCS-6 SiC fiber and the composite to determine the origin of the porosity and to characterize any further porosity developments which may occur when the material is subjected to thermal exposures.

The extent of fiber-matrix reaction was also characterized by SEM in the as-fabricated condition and at 815, 985, and 1200 °C for various times between 1 and 500 hr as shown in figure 14. The 815 and 985 °C temperatures within the $\alpha_2 + \beta$ region were chosen to begin to outline a suitable use regime for this composite based on fiber-matrix reaction and microstructural stability. The 1200 °C temperature was chosen so as to characterize the use limit of the composite based on fiber-matrix compatibility should over-temperature exposures be experienced. Note that these measurements are slightly less than the 985 and 1200 °C data published earlier on this composite (ref. 13). The present measurements were obtained at a much higher resolution and from metallographic mounts which were flatter than those used previously. Thus, the measurements of figure 14 are deemed more accurate. In all cases, the reaction zone was observed to grow in toward the fiber, as will be shown by the depletion of the C-rich coating of the SiC fiber, as well as outward in the direction of the matrix. The results at 815 and 985 °C over the entire time regime investigated and for 1200 °C after 10 hr were parabolic with time as would be expected from a diffusion controlled reaction. At 815 and 985 °C the reaction grew relatively slowly, exhibiting reaction rates of 5.42×10^{-2} μm/hr$^{1/2}$ at 815 °C and 3.35×10^{-1} μm/hr$^{1/2}$ at 985 °C. At 1200 °C, the fiber-matrix reaction rate accelerated to 2.38 μm/hr$^{1/2}$ between 10 and 100 hr exposure.

There are a couple of differences between the 815 and 985 °C data and the 1200 °C data which need to be mentioned. First, there is expected to be a difference in phases present based on the phase diagram of the matrix as shown previously in figure 2. This phase diagram of Ti_3Al-Nb (ref. 2) places the β transus temperature at approximately 1000 °C for Ti_3Al plus 11 at % (21 wt %) Nb. More recent work by Marquardt and Wasielewski (ref. 21) places the β transus temperature of the matrix at 1114 °C using their equation given below in °F, followed by conversion to °C:

$$\beta \text{ Transus Temperature (°F)} = 1775 \text{ °F} + 16.9° \text{ F/at \% Al} - 13 \text{ °F/at \% Nb}$$

$$-15.6 \text{ °F/at \% Ta} - 22.4 \text{ °F/at \% V.}$$

Thus, at 815 and 985° C, the matrix is the desired two-phase ordered $\alpha_2 + \beta$ structure and at 1200 °C the matrix is single phase, unordered β. Since diffusion in unordered β is anticipated to be faster than in ordered α_2 (ref. 22), diffusion rates within the matrix are expected to alter the fiber-matrix reaction growth somewhat. However, the overall rate controlling step is probably diffusion through the reaction zone at all three temperatures.

The second difference between the data at 815 and 985 °C compared to that at 1200 °C is the degree of protection offered by the C-rich coating of the SCS-6 SiC fiber. At the lower temperatures of 815 and 985 °C for all the

times investigated and at 1200 °C for 1 and 5 hr, some C-rich coating remained unreacted on the fiber and the reaction rates were relatively slow. The presence of the unreacted C-rich coating is illustrated in figure 15 for the composite annealed at 815 °C for 500 hr. By contrast, the sudden acceleration of reaction growth at 1200 °C and 10 hr was accompanied by complete reaction of the C-rich coating as shown in figure 16.

The complete analysis of the C-rich coating thickness at each temperature and time is plotted in figure 17. The quantity of C-rich coating remaining on the fiber in the as-fabricated condition is plotted at zero time. The double-pass SCS-6 SiC fiber used here had two layers of C-rich coating on the SiC surface which was approximately 3.4 μm thick as-fabricated in the composite. At 815 °C, the depletion of the C-rich coating followed a parabolic time dependence, with 2.9 μm of the C-rich coating remaining to protect the fiber even after 500 hr. At 985 °C, the C-rich coating was present at a thickness of approximately 3 μm through 10 hr, after which time a large drop in C-rich coating thickness was observed. The reaction of the C-rich coating at 1200 °C was exceedingly fast, being completely consumed after only 10 hr. The depletion of the C-rich coating is evidence that the fiber-matrix reaction zone is growing in toward the fiber, in addition to its outward growth into the matrix, since the dimensions of the SiC fiber only changed within the C-rich coating.

One other microstructural feature which was characterized was the growth of the β depleted region within the $\alpha_2 + \beta$ matrix adjacent to the fiber, as shown in figure 18. Again, the depletion zone thickness was parabolic with time at 815 and 985 °C, as would be expected for diffusion controlled reactions, with β depletion rates of 5.16×10^{-1} μm/hr$^{1/2}$ at 815 °C and 1.53 μm/hr$^{1/2}$ at 985 °C. The width of the β depleted zone was quite large after fabrication at an average of 4.27 μm. After 500 hr at 815 °C, the average β zone was 15.17 μm thick and after 100 hr at 985 °C, it was an average of 18.24 μm thick, which resulted in regions between fibers which were largely devoid of β as shown in figures 19(a) and (b). As was previously discussed, the addition of Nb and the retention of β was necessary for the realization of ductility in this Ti$_3$Al based matrix. Thus, it is reasonable to predict that this depletion of second phase within the matrix adjacent to the fiber will degrade the composite mechanical properties in the same manner as a brittle fiber-matrix reaction zone (ref. 23) and should be treated as such. Therefore, a more realistic view of the quantity of the fiber-matrix interface would show a combined thickness of the fiber-matrix reaction zone and the depleted zones as have been plotted in figure 20. Figures 19 and 20 point out the complexities involved in designing an intermetallic matrix composite. A minimal and stable fiber-matrix reaction zone is desired as well as a stable matrix microstructure, particularly when two or more phases are required for ductility within the intermetallic matrix.

E. Fiber and Matrix Coefficients of Thermal Expansions

One final area of importance in intermetallic matrix composites is the large difference in CTE which currently exists between available fibers and candidate intermetallic matrices. This two- to fourfold difference in CTE is illustrated in figure 21 for SiC fiber (ref. 11), W (ref. 24), Al$_2$O$_3$ fiber (ref. 14), Ti-24Al-11Nb (Unpublished research by P.W. Angel, R. Hann, and P.K. Brindley of Lewis), NiAl (ref 25), and FeAl (ref. 25). The stresses induced by a CTE mismatch during cooling from elevated temperatures can be

detrimental, particularly when the intermetallic matrix exhibits limited ductility; and can cause cracks to develop. We observed such cracks in SiC/Ti-24Al-11Nb when the samples were accruing time at temperature for the previously discussed reaction studies, and in the process were cycled several times from elevated temperature to room temperature. An example is shown in figure 22, in which the composite was annealed at 985 °C for 10 hr, underwent 3 cycles from 985 °C to room temperature, and developed cracks. The cracks appear to have originated near the fiber-matrix interface and to have progressed outward through the β depleted zone in the matrix.

Futhermore, large differences in CTE would also be expected to result in fiber-matrix debonding if the strain induced at the interface exceeded its strain-to-failure as discussed previously. Such debonding and resulting fiber pullout as were observed on the tensile fracture surfaces of this composite may prove to be beneficial in terms of fracure toughness of the composite but in general are not desired if full fiber strenghthening is to be realized. Thus, the need for some avenue of reducing the effect of large CTE differences between fibers and matrices is pointed out. This is especilly pertinent when low matrix ductility limits its ability to absorb the CTE-induced strain without detrimental effects to the mechanical properties of the composite.

SUMMARY OF RESULTS

1. Fully consolidated SiC/Ti-24Al-11Nb composites were fabricated using a powder cloth technique. Control of unwanted trace elements appears feasible with this technique.

2. Microfocus radiography was found useful in detecting fiber breakage, large regions of porosity, and for mapping out regions for specimen preparation from the composite plates.

3. Tensile properties of the composite were near ROM-predicted values at intermediate temperatures with negative departures from ROM at 23 °C and above 650 °C. At 23 °C, lack of matrix ductility with subsequent crack propagation through the brittle fibers is proposed as the reason for this departure. At higher temperatures, the departure from ROM appears to result from a weak fiber-matrix bond, defined as one which could not withstand the combination of imposed tensile stresses and stresses induced by the fiber-matrix CTE mismatch.

4. As-fabricated reaction zone products of $(Ti,Nb)C$; $(Ti,Nb)_3 AlC$; and $(Ti,Nb)_5Si_3$ were identified. Porosity was observed within the $(Ti,Nb)C$, some of which may correspond to the original fiber-matrix interface before consolidation.

5. Characterization of reaction zone, C-rich coating, and β depletion zone indicated consideration of the effects of all three regions on mechanical properties will be necessary to determine composite use temperature and life.

6. Thermal cycling of the high oxygen-containg SiC/Ti-24Al-11Nb (at %) composite resulted in the formation of cracks at the fiber-matrix interface which extended into the matrix. This points to the need to reduce the fiber-matrix CTE mismatch, especially when low matrix ductility limits the ability to absorb the induced strain.

REFERENCES

1. Stephens, J.R.: High Temperature Metal Matrix Composites for Future Aerospace Systems. NASA TM-100212, 1987.

2. Alisova, S.P.; and Budberg, P.B.: Phase Diagrams of Metallic Systems, Vol. 16, Viniti Press, Moscow, 1970.

3. Lipsitt, H.A.: Titanium Aluminides - An Overview. High-Temperature Ordered Intermetallic Alloys, MRS Symp. Proc. Vol. 39, C.C. Koch, C.T. Liu, and N.S. Stoloff, eds., Materials Research Society, 1985, pp. 351-364.

4. Martin, P.L., et al.: The Effects of Alloying on the Microstructure and Properties of Ti_3Al and TiAl. Titanium '80 Science and Technology, Vol. 2, H. Kimura and O. Izumi, eds., The Metallurgical Society, PA, 1980, pp. 1245-1254.

5. Moxson, V.S.; and Friedman, G.I.: Powder Metallurgy of Titanium Aluminides. Progress in Powder Metallurgy, Vol. 42, Metal Powder Industries Federation, 1986, pp. 489-500.

6. Yolton, C.F., et al.: Powder Metallurgy of Titanium Aluminide Components. Titanium: Rapid Solidification Technology, E.H. Froes and D. Eylon, eds., The Metallurgical Society of AIME, 1986, pp. 263-271.

7. Stoloff, N.S.; and Davies, R.G.: The Mechanical Properties of Ordered Alloys. Prog. Mater. Sci., vol. 13, no. 1, 1966, pp. 3-84.

8. Lipsitt, H.A.; Schechtman, D.; and Schafrik, R.E.: The Deformation and Fracture of Ti_3Al at Elevated Temperatures. Metall. Trans. A, vol. 11, no. 8, Aug. 1980, pp. 1369-1375.

9. Sastry, S.M.L.; and Lipsitt, H.A.: Plastic Deformation of TiAl and Ti_3Al. Titanium '80 Science and Technology, vol. 2, H. Kimura and O. Izumi, eds., The Metallurgical Society of AIME, 1980, pp. 1231-1243.

10. Schulson, E.M.: The Effects of Grain Size on the Flow and Fracture of Long-Range Ordered Alloys. High-Temperature Ordered Intermetallic Alloys, MRS Symp. Proc. Vol. 39, C.C. Koch, C.T. Liu, and N.S. Stoloff, eds., Materials Research Society, 1985, pp. 193-204.

11. DiCarlo, J.A.: Creep of Chemically Vapour Deposited SiC Fibres. J. Mater. Sci., vol. 21, no. 1, Jan. 1986, pp. 217-224.

12. DiÇarlo, J.A.: Fibers for Structurally Reliable Metal and Ceramic Composites. J. Met., vol. 37, no. 6, June 1985, pp. 44-49.

13. Brindley, P.K.: SiC Reinforced Aluminide Composites. High-Temperature Ordered Intermetallic Alloys II, MRS Symp. Proc. Vol. 81, N.S. Stoloff, et al., eds., Materials Research Society, 1987, pp. 419-424.

14. Lewis, G.K. Jr.; and Romine, J.C.: A New High Temperature Ceramic Fiber. Presented at the 32nd SAMPE Symposium, Anaheim, CA, Apr. 7, 1987.

15. Petrasek, D.W.: High-Temperature Strength of Refractory-Metal Wires and Consideration for Composite Applications. NASA TN D-6881, 1972.

16. Klima, S.J.; Baaklini, G.Y.; and Abel, P.B.: Nondestructive Evaluation of Structural Ceramics. NASA TM-88978, 1987.

17. Kirchoff, S.D.; and Adkins, J.Y.: Thinning of Aluminum Powder Particles for Transmission Electron Microscopy. Metallography, vol. 20, no. 1, Feb. 1987, pp. 75-87.

18. Stoloff, N.S.; and Davies, R.G.: The Mechanical Properties of Ordered Alloys. Prog. Mater. Sci., vol. 13, no. 1, 1966, pp. 3-84.

19. Levitt, A.P.: Stresses in Metal Matrix Composites due to Fiber Matrix Thermal Expansion Mismatch. Ceram. Eng. Sci. Proc., vol. 1, no. 7-8, July-Aug. 1980, pp. 419-423.

20. Baumann, S.F.; and Brindley, P.K.: Reaction Zone Microstructure in a Ti_3Al + Nb/SiC Composite. Presented at the 1988 TMS Fall Meeting, Sept. 26-29, Chicago, IL, 1988.

21. Marquardt, B.J.; and Wasielewski, G.E.: Alloying Element Effect on the Beta Transus Temperature of Alpha-Two Titanium Aluminide. Presented at the 1987 Fall TMS Meeting, Cincinnati, OH, Oct. 1987.

22. Bakker, H., et al.: Defects, Disordering and Mobility in Intermetallic Compounds. Diffusion in Solids: Recent Developments, M.A. Dayananda and G.E. Murch, eds., The Metallurgical Society of AIME, 1985, pp. 39-65.

23. Shorshorov, M.Kh., et al.: Brittle Interface Layers and the Tensile Strength of Metal-Matrix Fibre Composites. J. Mater. Sci., vol. 14, no. 8, Aug. 1979, pp. 1850-1861.

24. Touloukian, Y.S., et al., eds.: Thermophysical Properties of Matter, vol. 12, Thermal Expansion - Metallic Elements and Alloys, IFI/Plenum Co., New York, 1977, p. 355.

25. Clark, R.W.; and Whittenberger, J.D.: Thermal-Expansion of Binary CoAl, FeAl, and NiAl Alloys. Thermal Expansion 8, T.A. Hahn, ed., Plenum Press, 1984, pp. 189-196.

TABLE I. – CHEMISTRIES OF BOTH THE FIRST (HIGH OXYGEN) AND SECOND (LOW OXYGEN)

GENERATION OF PREALLOYED POWDERS AND AS–FABRICATED COMPOSITES

(a) Atomic percent

	Ti	Al	Nb	O	C	H	N	F
Prealloyed Ti–24Al–11Nb powder (high oxygen)	60.7	25.6	13.1	0.332	0.044	0.190	0.010	-------
As–fabricated SiC/Ti–24Al–11Nb (high oxygen)	60.9	24.9	13.2	0.453	0.129	0.288	0.066	0.0069
Prealloyed Ti–24Al–11Nb powder (low oxygen)	65.2	23.9	10.3	0.175	0.043	0.424	0.014	-------
As–fabricated SiC/Ti–24Al–11Nb (low oxygen)	63.9	24.1	11.5	0.206 to 0.221	0.123	0.095	0.004	<0.0025 to 0.0040

(b) Weight percent

	Ti	Al	Nb	O	C	H	N	F
Prealloyed Ti–24Al–11Nb powder (high oxygen)	60.3	14.3	25.3	0.11	0.011	0.004	0.003	-------
As fabricated SiC/Ti–24Al–11Nb (high oxygen)	60.4	13.9	25.4	0.15	0.032	0.006	0.019	0.0027
Prealloyed Ti–24Al–11Nb powder (low oxygen)	65.8	13.6	20.1	0.059	0.011	0.009	0.004	-------
As fabricated SiC/Ti–24Al–11Nb (low oxygen)	64.0	13.6	22.3	0.069 to 0.074	0.031	0.002	0.012	<0.001 to 0.0016

TABLE II. – ELASTIC MODULUS VALUES OF

SiC/Ti–24Al–11Nb AT ROOM TEMPERATURE

AND 425 °C

[35 to 40 vol % SiC/Ti–24Al–11Nb]

Test temperature	23 °C	425 °C
Elastic modulus, GPa	199 226 236	197 219 ---
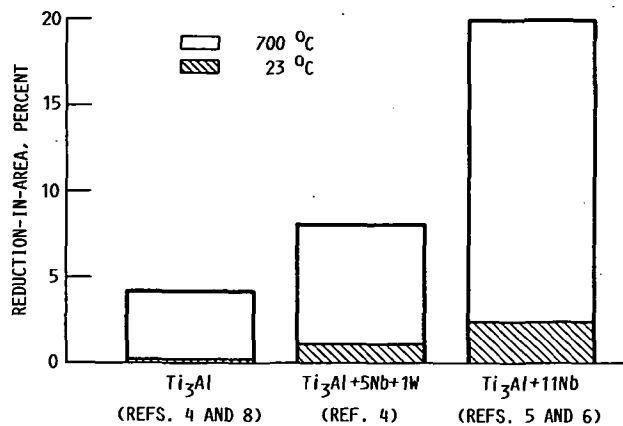
FIGURE 1. - REDUCTION-IN-AREA OF Ti_3Al AND Ti_3Al WITH
INCREASING AMOUNTS OF Nb (AT. %) AT ROOM TEMPERATURE
AND AT 700 °C (REFS. 4, 5, 6, AND 8).
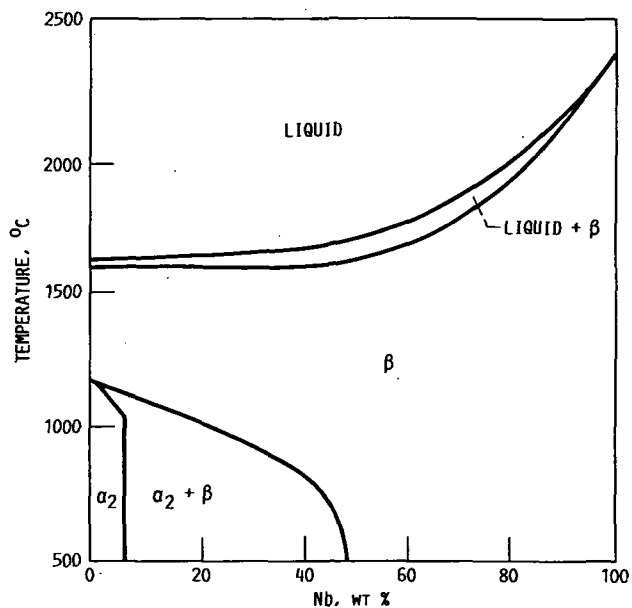
FIGURE 2. - PSEUDOBINARY PHASE DIAGRAM OF Ti_3Al-Nb
(REF. 2).

FIBER	TEST ENVIRONMENT	FIBER DIAMETER, μM	REFERENCE
——— SCS-6 SiC	Ar, N_2[a]	140	12
– – – SCS-6 SiC	O_2[a]	140	12
······· SCS-6 SiC	He, AIR	140	13
–·–· Al_2O_3-ZrO_2	AIR[a]	20	14
–··–·· SINGLE CRYSTAL Al_2O_3	AIR	254	(b)
–····–···· FP Al_2O_3	AIR[a]	20	14
–·–·– W-Re-Hf-C	He	380	15

[a]EXPOSED TO ENVIRONMENT AT TEMPERATURE. TENSILE TESTED
AT 23 °C (ALL OTHERS TENSILE TESTED AT TEMPERATURE).
[b]M. JASKOWIAK, UNPUBLISHED.
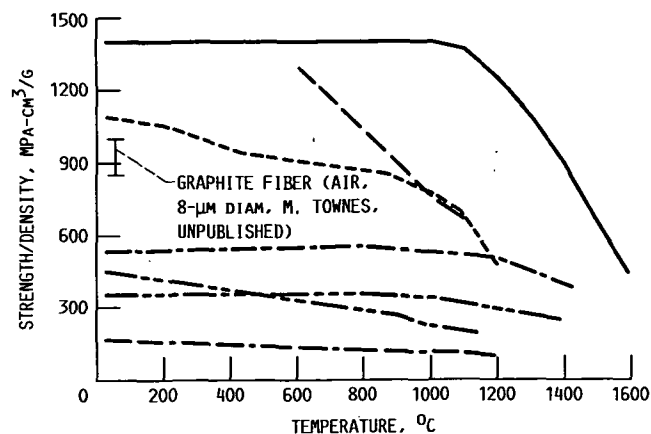
FIGURE 3. - STRENGTH/DENSITY COMPARISON OF CURRENTLY
AVAILABLE CONTINUOUS FIBERS.

14
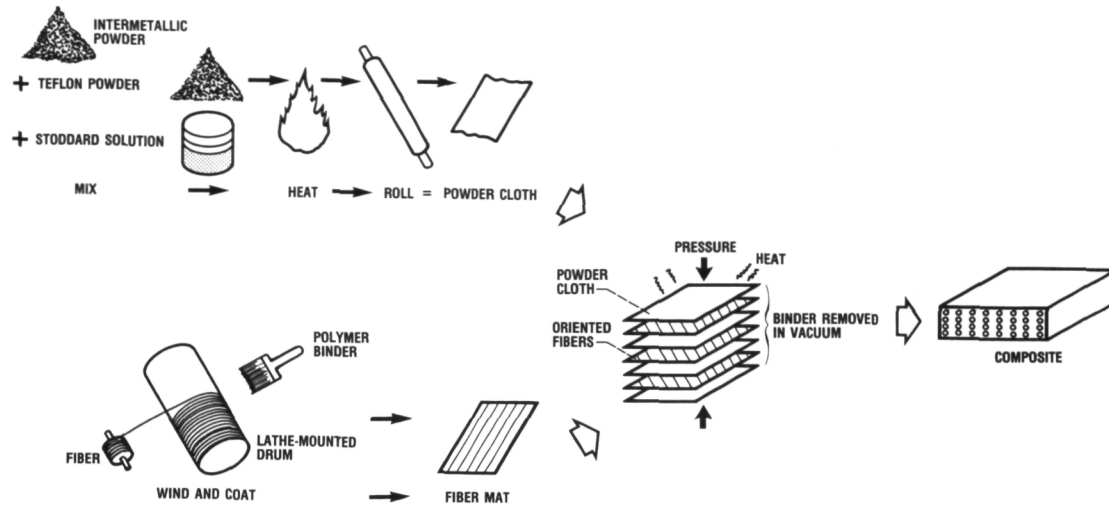
FIGURE 4. – SCHEMATIC OF POWDER CLOTH TECHNIQUE USED IN FABRICATION OF SiC/Ti-24Al-11Nb COMPOSITES.
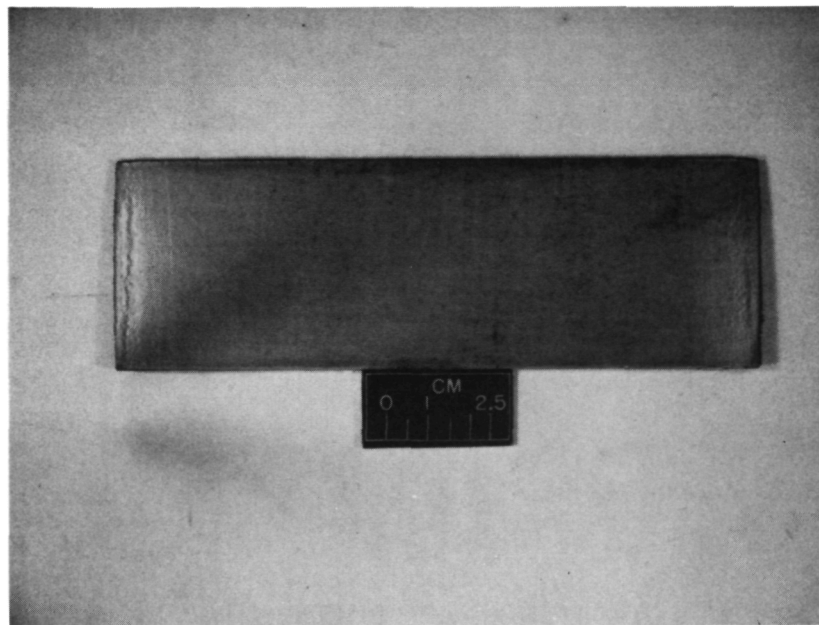
FIGURE 5. – TYPICAL SiC/Ti-24Al-11Nb COMPOSITE PLATE FABRICATED BY POWDER CLOTH TECHNIQUE.
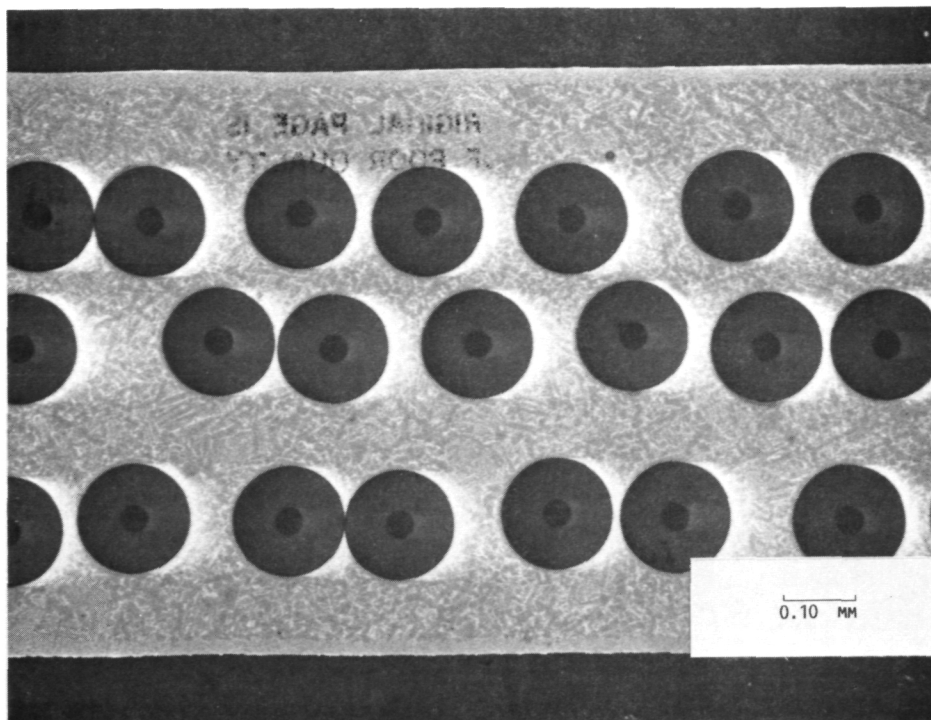
FIGURE 6. – TRANSVERSE SECTION DEPICTING FIBER DISTRIBUTION AND FULL MATRIX CONSOLIDATION IN AS-FABRICATED SiC/Ti-24Al-11Nb COMPOSITE (10-μm CLADDING ON OUTER SURFACES OF COMPOSITE MECHANICALLY REMOVED BEFORE TESTING).
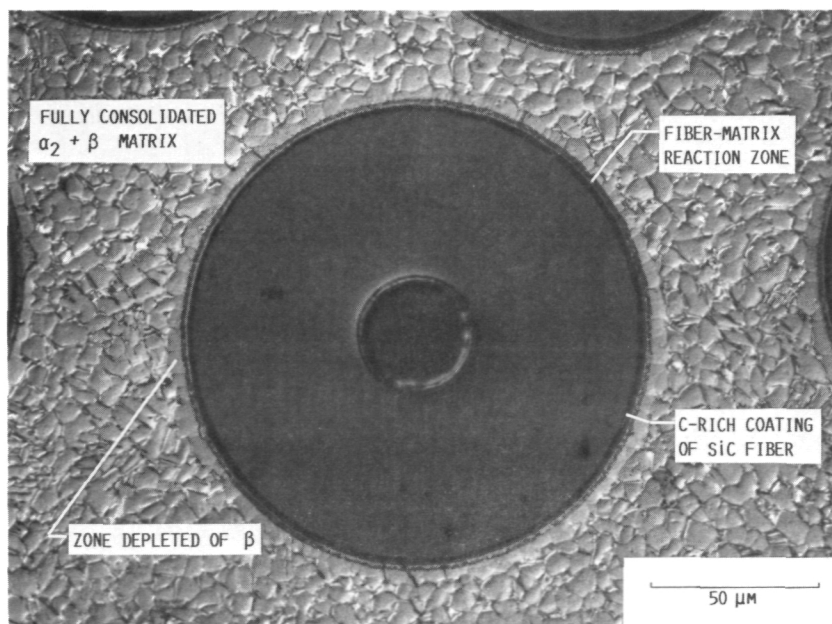
FIGURE 7. – AS-FABRICATED SiC/Ti-24Al-11Nb COMPOSITE SHOWING TWO-PHASE α_2 (MAJOR PHASE) + β (MINOR PHASE) MATRIX, ZONE DEPLETED OF β ENCIRCLING FIBER, 2-μM FIBER-MATRIX REACTION ZONE, AND C-RICH COATING PRESENT ON AS-RECEIVED SCS-6 SiC FIBER.
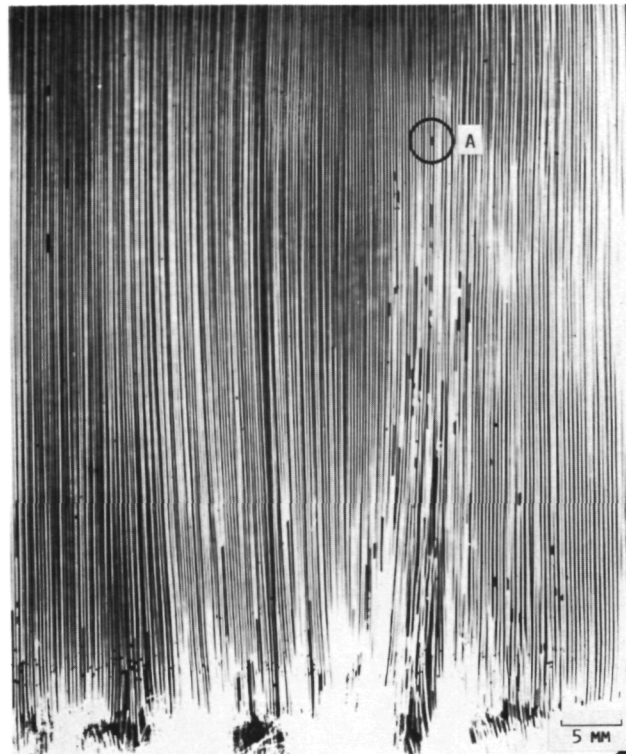
FIGURE 8. - MICROFOCUS RADIOGRAPH OF ONE END OF THREE-FIBER PLY
SiC/Ti-24Al-11Nb COMPOSITE. AREAS SUCH AS A ARE BROKEN
FIBERS (VERTICAL WHITE BANDS) WITH MATING FRACTURE SURFACES
SEPARATED BY DARK REGION IN WHICH MATRIX APPARENTLY INFILTRATED
DURING CONSOLIDATION.
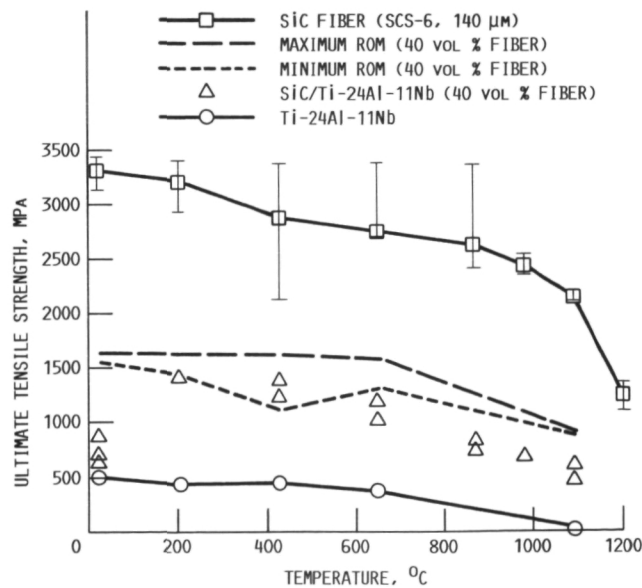
FIGURE 9. - ULTIMATE TENSILE STRENGTH AT TEMPERATURE FOR
SiC FIBER (WITH MAXIMUM AND MINIMUM VALUES INDICATED
BY SCATTER BANDS), Ti-24Al-11Nb MATRIX, AND 40 VOL %
SiC/Ti-24Al-11Nb COMPOSITE COMPARED WITH RULE OF MIX-
TURES (ROM).

17
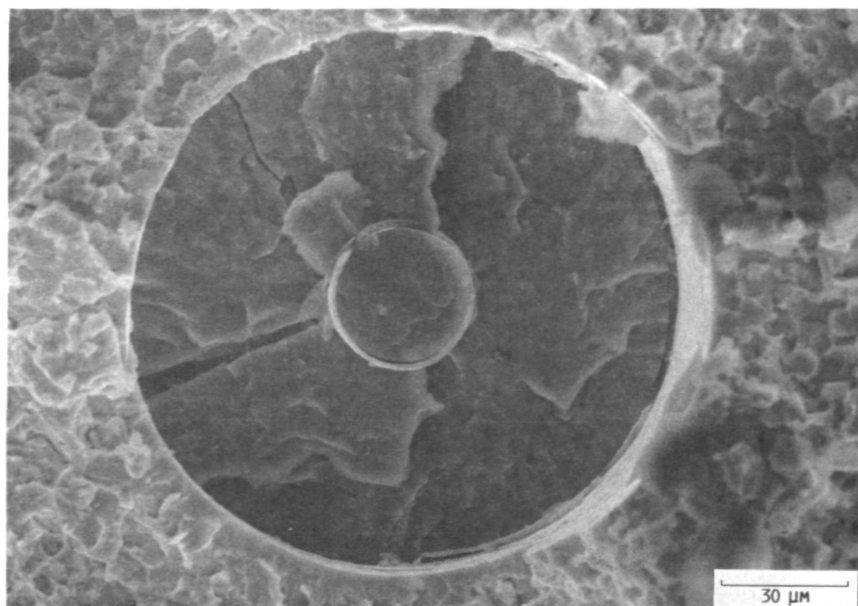
(a) 23 °C.
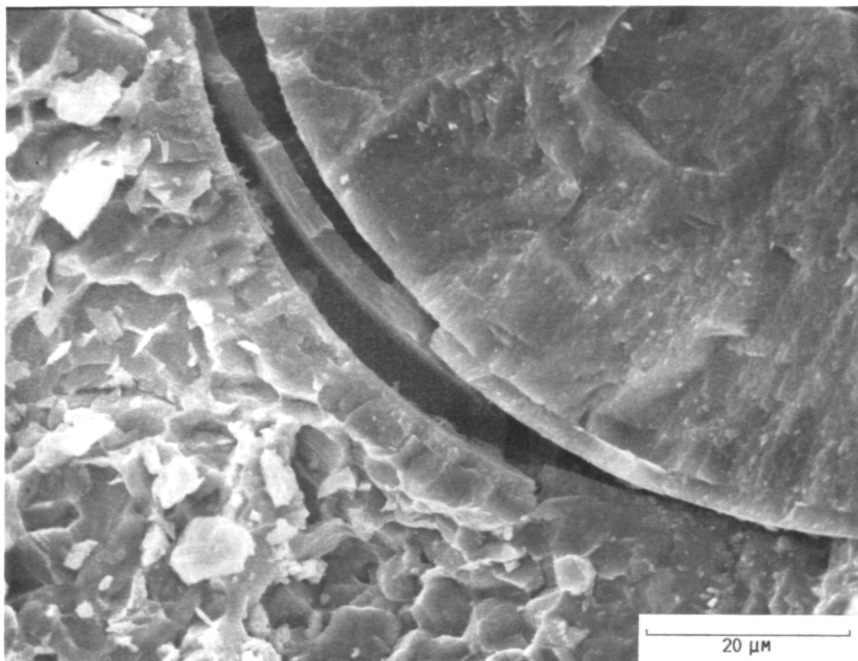
(b) 650 °C.

FIGURE 10. – SiC/Ti-24Al-11Nb FRACTURE SURFACES AT VARIOUS TEMPERATURES SHOWING DEBONDING
AT ELEVATED TEMPERATURES AT FIBER/FIBER COATING INTERFACE AND AT FIBER COATING/MATRIX
INTERFACE.

18
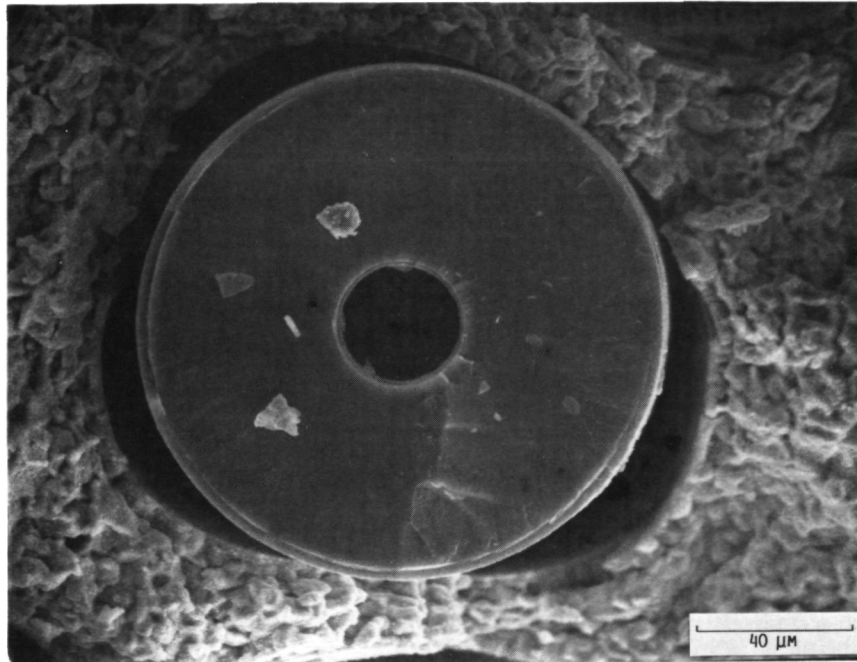
(c) 1100 °C.

FIGURE 10. – CONCLUDED.
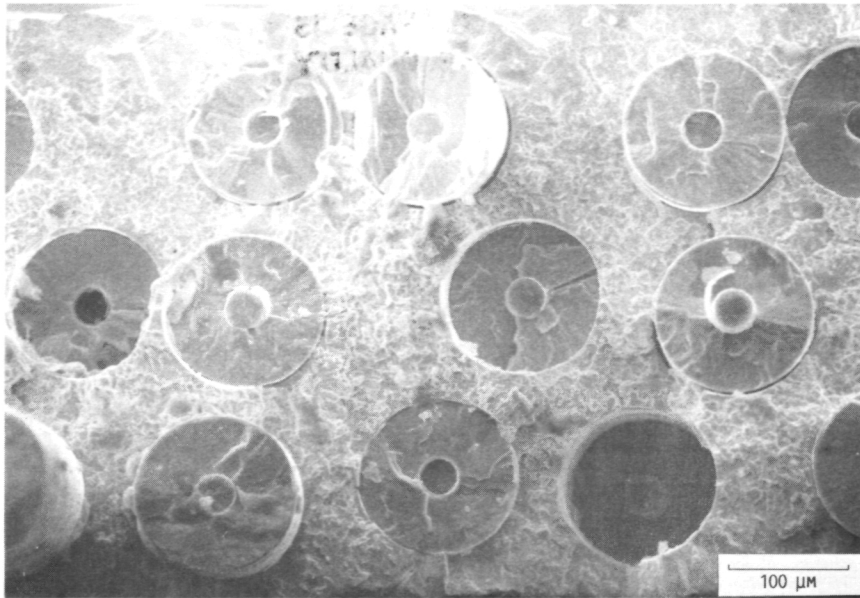
(a) 23 °C).
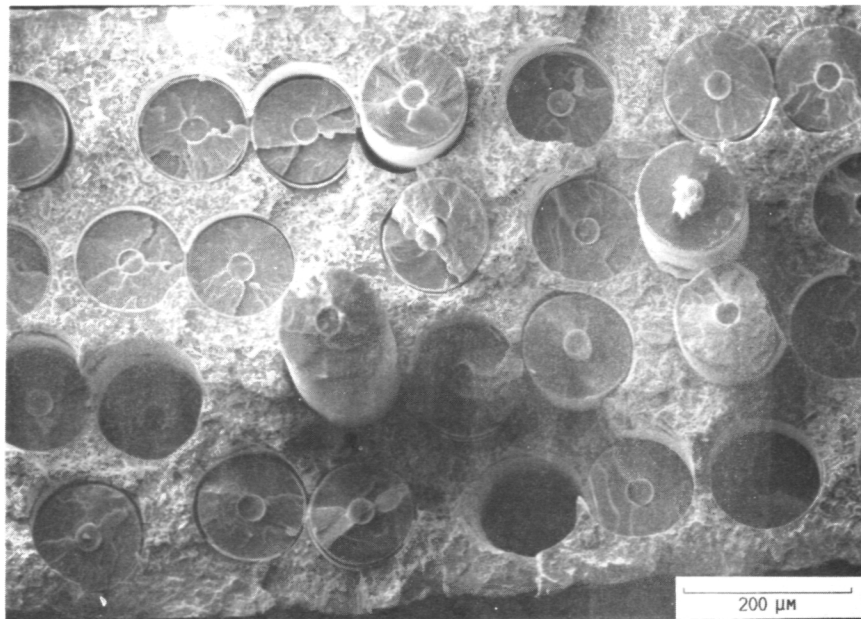
(b) 425 °C.

FIGURE 11. - SiC/Ti-24Al-11Nb FRACTURE SURFACES AT VARIOUS TEMPERATURES SHOWING INCREASED
AMOUNTS OF FIBER PULLOUT WITH INCREASED TEST TEMPERATURE.
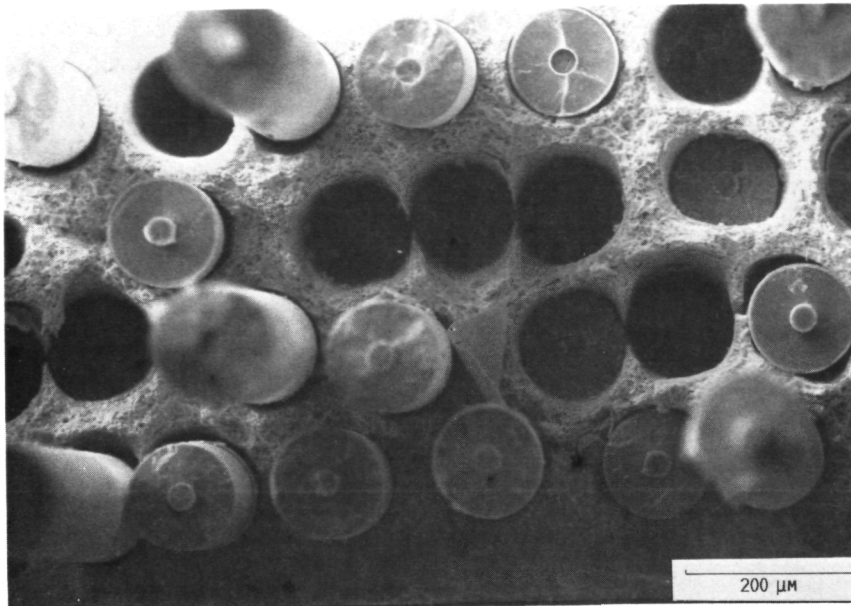
(c) 875 °C.
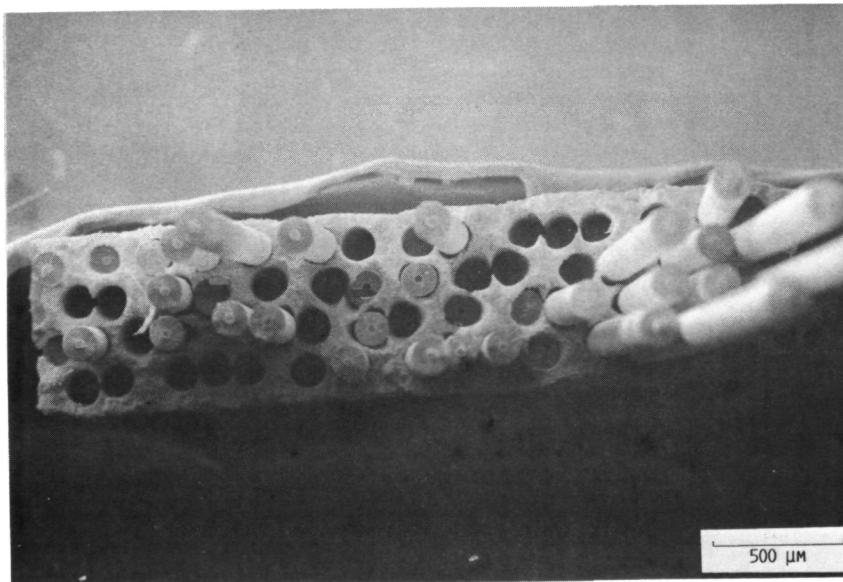
(d) 1100 °C.

FIGURE 11. – CONCLUDED.
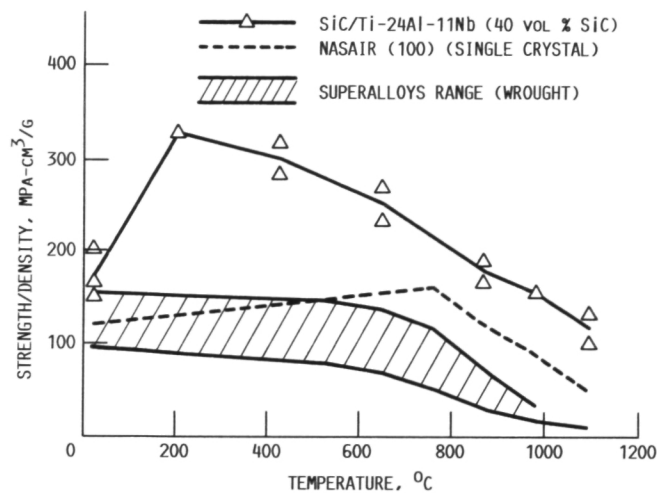
FIGURE 12. - STRENGTH/DENSITY COMPARISON OF 0^0 SiC/Ti-24Al-11Nb COMPOSITE WITH Ni-BASE SUPERALLOYS.

ZONE 1	(Ti,Nb)C (CUBIC, 1.5 μM WIDE)
ZONE 2	(Ti,Nb)$_3$AlC (CUBIC, 1.8 μM WIDE)
BOTH ZONES	(Ti,Nb)$_5$Si$_3$
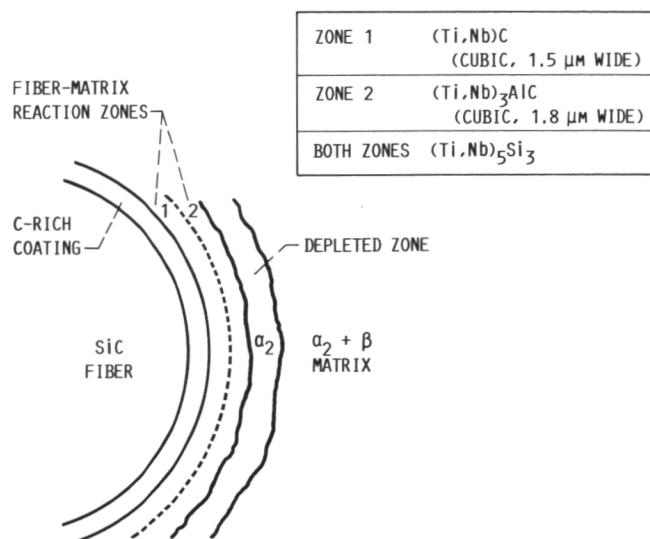
FIGURE 13. - SCHEMATIC OF STEM RESULTS OF AS-FABRICATED REACTION ZONE IN SiC/Ti-24Al-11Nb.
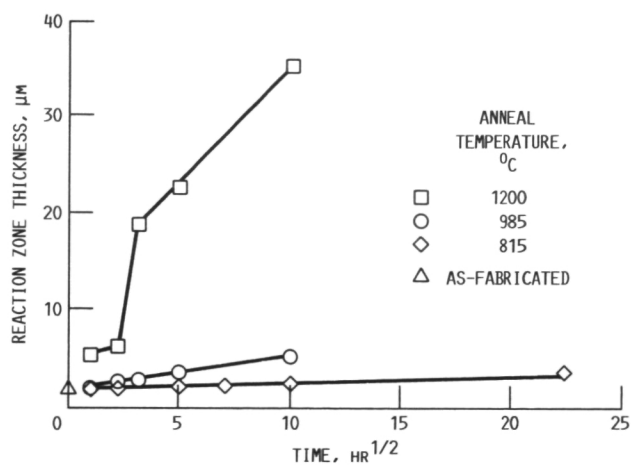
FIGURE 14. - SiC/Ti-24Al-11Nb FIBER-MATRIX REACTION ZONE THICKNESS IN AS-FABRICATED CONDITION AND AFTER ANNEALING (REACTION RATES, 5.42×10^{-2}, 3.35×10^{-1}, AND 2.38 μM/HR$^{1/2}$ AT 815, 985, AND 1200 ^{0}C, RESPECTIVELY; MAXIMUM ERROR, ±5.4 PERCENT AT 95 PERCENT CONFIDENCE LEVEL).
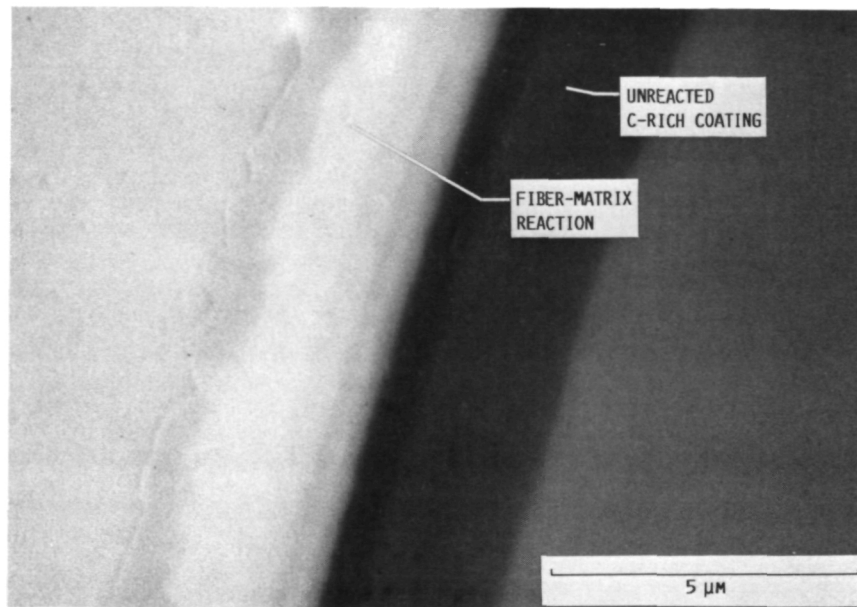
FIGURE 15. – UNREACTED C-RICH COATING REMAINING ON SSC-6 SiC FIBER AFTER SiC/Ti-24Al-11Nb COMPOSITE HAS BEEN ANNEALED AT 815 °C FOR 500 HR.
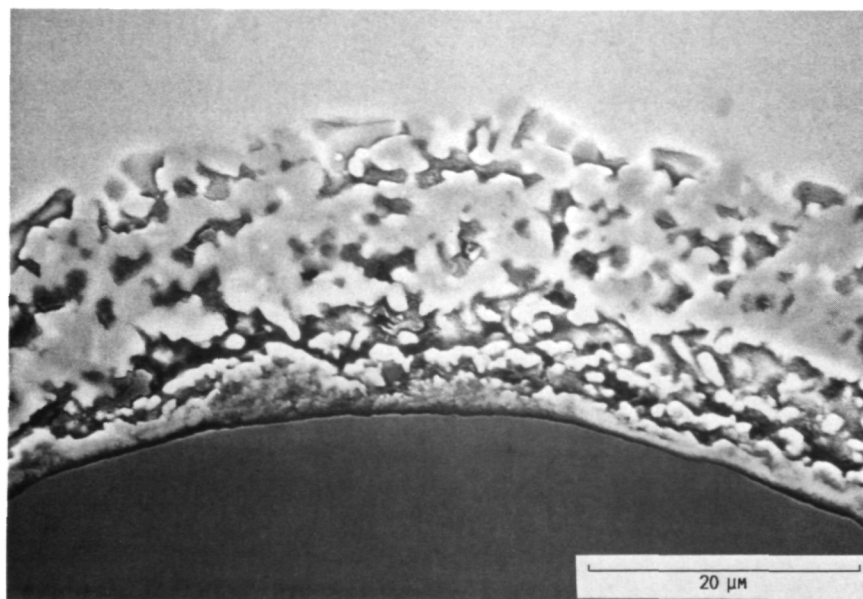
FIGURE 16. – C-RICH COATING COMPLETELY REACTED WITH Ti-24Al-11Nb MATRIX AFTER ANNEALING AT 1200 °C FOR 10 HR (CORRESPONDS TO SUDDEN ACCELERATION OF FIBER-MATRIX REACTION GROWTH).
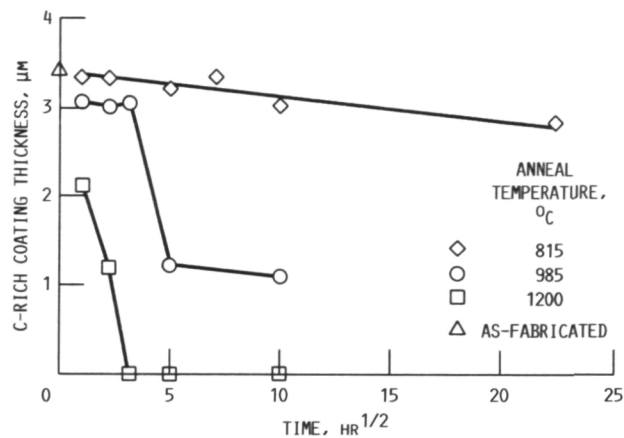
FIGURE 17. - C-RICH COATING THICKNESS REMAINING ON SCS-6
SiC FIBER UPON FABRICATION OF SiC/Ti-24Al-11Nb COMPOS-
ITE AND AFTER ANNEALING (C-RICH COATING REACTION RATE,
2.36×10^{-2} $\mu M/HR^{1/2}$ AT 815 °C; MAXIMUM ERROR, ±5.4 PER-
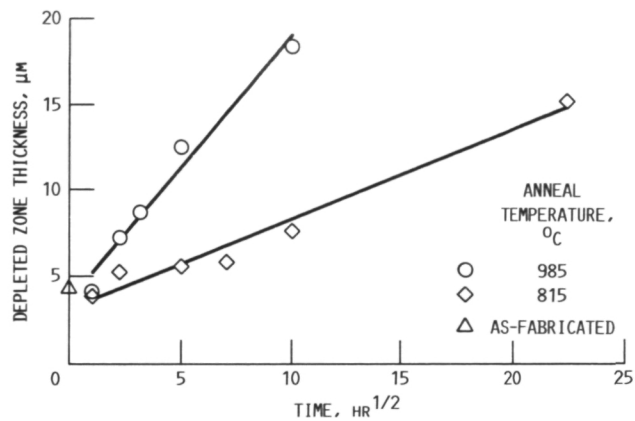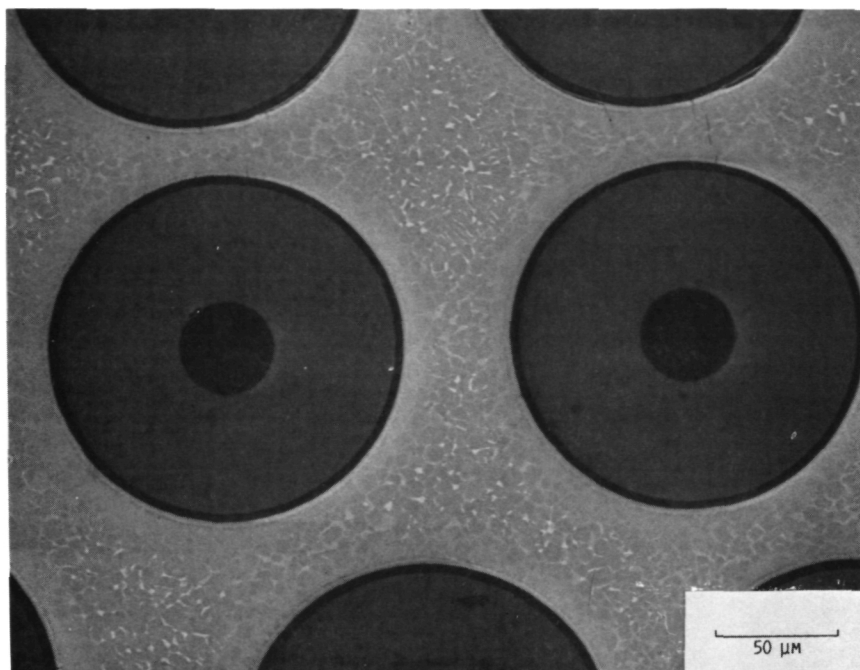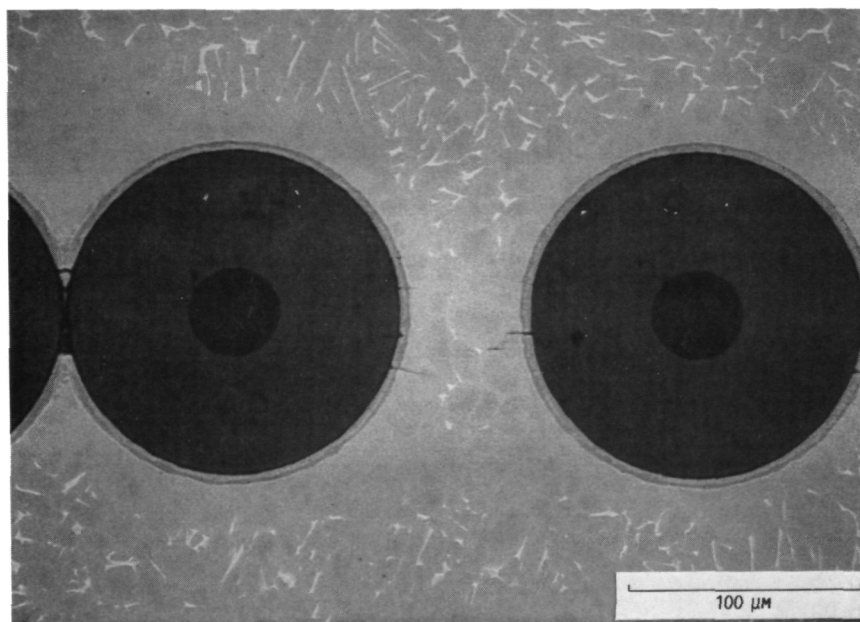CENT AT 95 PERCENT CONFIDENCE LEVEL).

FIGURE 18. - THICKNESS OF ZONE IMMEDIATELY ADJACENT TO FIBER
WITHIN MATRIX WHICH WAS DEPLETED OF β PHASE (β DEPLETION
RATES, 5.16×10^{-1} $\mu M/HR^{1/2}$ AT 815 °C AND 1.53 $\mu M/HR^{1/2}$ AT
985 °C; MAXIMUM ERROR, ±6.4 PERCENT AT 95 PERCENT CONFIDENCE
LEVEL).

(a) 815 °C/500 HR.

(b) 985 °C/100 HR.

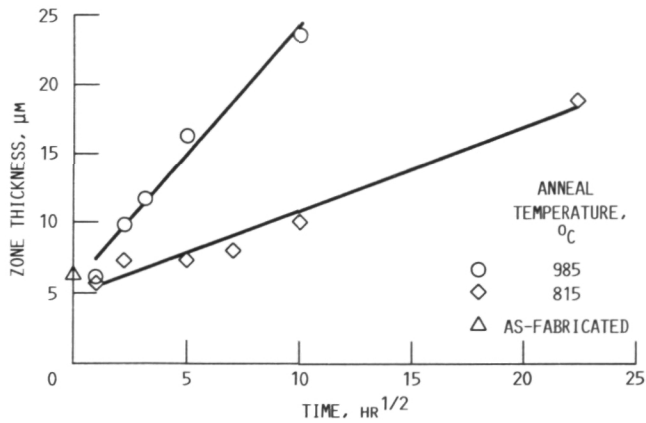FIGURE 19. — β DEPLETION ZONES AROUND FIBERS IN SiC/Ti-24Al-11Nb AFTER ANNEALING.

FIGURE 20. - SUMMATION OF REACTION AND β DEPLETION ZONES IN SiC/Ti-24Al-11Nb (REACTION PLUS β DEPLETION RATES, 6.1×10^{-1} $\mu M/HR^{1/2}$ AT 815 °C AND 1.87 $\mu M/HR^{1/2}$ AT 985 °C; MAXIMUM ERROR, ±5.6 PERCENT AT 95 PERCENT CONFIDENCE LEVEL).
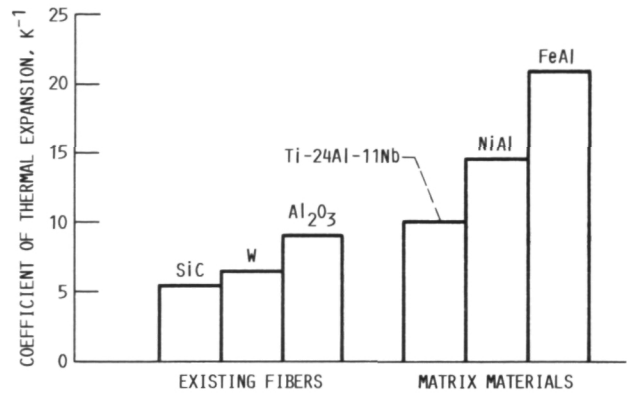

FIGURE 21. - COMPARISON OF COEFFICIENTS OF THERMAL EXPANSION AT 973 K FOR CURRENTLY AVAILABLE FIBERS AND SOME CANDIDATE MATRIX MATERIALS.
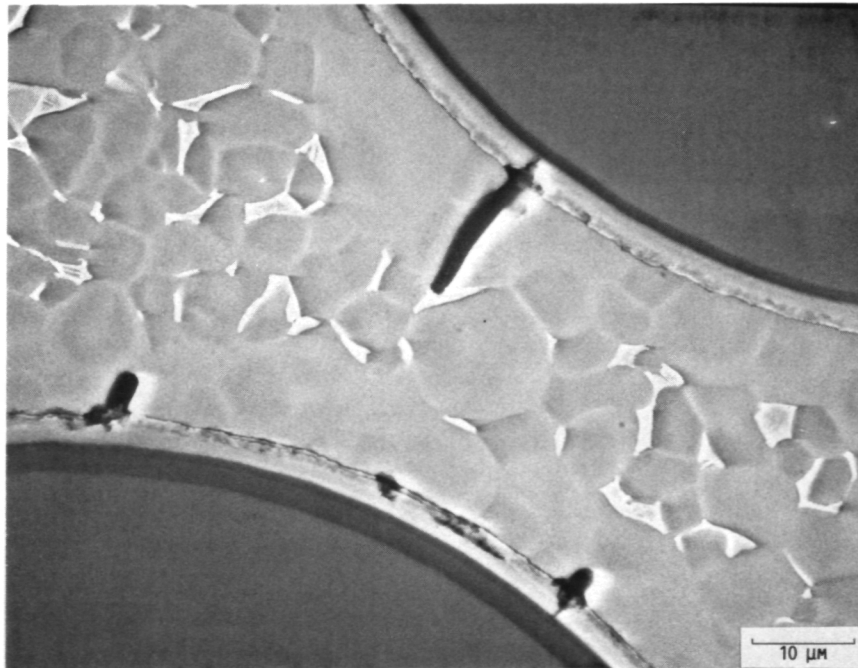

FIGURE 22. - CRACKS FORMED IN SiC/Ti-24Al-11Nb AFTER THREE THERMAL CYCLES FROM 985 °C TO ROOM TEMPERATURE.

Report Documentation Page

1. Report No. NASA TM-100956	2. Government Accession No.	3. Recipient's Catalog No.
4. Title and Subtitle Investigation of SiC/Ti-24Al-11Nb Composite		5. Report Date 6. Performing Organization Code
7. Author(s) P.K. Brindley, P.A. Bartolotta, and S.J. Klima		8. Performing Organization Report No. E-4253 10. Work Unit No. 505-63-01
9. Performing Organization Name and Address National Aeronautics and Space Administration Lewis Research Center Cleveland, Ohio 44135-3191		11. Contract or Grant No. 13. Type of Report and Period Covered Technical Memorandum
12. Sponsoring Agency Name and Address National Aeronautics and Space Administration Washington, D.C. 20546-0001		14. Sponsoring Agency Code

15. Supplementary Notes

16. Abstract

A summary of on-going research on the characterization of a continuous-fiber reinforced SiC/Ti-24Al-11Nb (at %) composite is presented. The powder metallurgy fabrication technique is described as are the nondestructive evaluation results of the as-fabricated composite plates. Tensile properties of the SiC fiber, the matrix material, and the 0° SiC/Ti-24Al-11Nb composite (fibers oriented unidirectionally, parallel to the loading axis) from room temperature to 1100 °C are presented and discussed with regard to the resultant fractography. The as-fabricated fiber-matrix interface has been examined by scanning transmission electron microscopy and the compounds present in the reaction zone have been identified. Fiber-matrix interaction and stability of the matrix near the fiber is characterized at 815, 985 and 1200 °C from 1 to 500 hr. Measurements of the fiber-matrix reaction, the loss of C-rich coating from the surface of the SiC fiber, and the growth of the β depleted zone in the matrix adjacent to the fiber are presented. These data and the difference in coefficient of thermal expansion between the fiber and matrix are discussed in terms of their likely effects on mechanical properties.

17. Key Words (Suggested by Author(s)) Titanium aluminide; Composites; Mechanical properties; Fiber-matrix reaction; Intermetallics	18. Distribution Statement Unclassified – Unlimited Subject Category 24

19. Security Classif. (of this report) Unclassified	20. Security Classif. (of this page) Unclassified	21. No of pages 28	22. Price* A03